Tone Stimulus Detection in Rats Using RRAM-Based Local Field Potential Monitoring

Citation for published version:
Sbandati, C, Stathopoulos, S, Foster, P, Peer, N, Serb, A, Wang, S, Cohen, D & Prodromakis, T 2024, Tone Stimulus Detection in Rats Using RRAM-Based Local Field Potential Monitoring. in *2023 IEEE Biomedical Circuits and Systems Conference (BioCAS).* IEEE Biomedical Circuits and Systems (BIOCAS) , IEEE, Artificial Intelligence BioMedical Circuits And Systems For Health, Toronto, Ontario, Canada, 19/10/23. https://doi.org/10.1109/BioCAS58349.2023.10388917

Digital Object Identifier (DOI):
10.1109/BioCAS58349.2023.10388917

Link:
Link to publication record in Edinburgh Research Explorer

Document Version:
Peer reviewed version

Published In:
2023 IEEE Biomedical Circuits and Systems Conference (BioCAS)

Tone Stimulus Detection In Rats Using RRAM-Based Local Field Potential Monitoring

Caterina Sbandati*, Spyros Stathopoulos*, Patrick Foster*, Noam D. Peer†,
Alexantrou Serb*, Shiwei Wang*, Dana Cohen†, Themis Prodromakis*
*Institute for Integrated Micro and Nano Systems, School of Engineering, University of Edinburgh, EH9 3BF, UK
† The Gonda Brain Research Center, Bar-Ilan University, Ramat-Gan, 52900, Israel
Corresponding author email: c.a.l.sbandati@sms.ed.ac.uk

***Abstract*—The comprehension of brain activity presents significant challenges in the field of neuroscience. Contrary to spikes, Local Field Potentials (LFPs) present improved stability acquisition in chronic implant scenarios and potential reductions in sampling and processing rates. While existing electrophysiology acquisition systems focus predominantly on spike detection and sorting, there is a lack of real-time tools for exploiting LFPs. To address this gap, we present a Resistive-RAM (RRAM) based approach to process LFP traces. Our method follows an improved Memristive Integrating Sensor (MIS) protocol to effectively detect LFP events recorded from the deep-brain of an awake rat, while externally stimulated by a tone. Experimental results demonstrate the feasibility of real-time neural activity processing, offering insights into detecting meaningful external stimuli and facilitating efficient neural state estimation.**

***Index Terms*—RRAM, bio-signal processing, edge processing, local field potential (LFP), memristor, real-time detection**

I. Introduction

Gaining meaningful insights from brain activity remains a highly complex and challenging problem. Neural recording techniques play a crucial role in elucidating the principles of brain function. A fundamental trade-off exists between invasiveness and resolution, spanning from non-invasive electroencelography (EEG) down to deep brain intracranial recording. Spike detection with invasive implants is currently popular, as it gives highly detailed information, up to single neuron activity [1]. However, recent studies investigating Local Field Potentials (LFPs) have directed interest in their advantageous effects in comparison to spikes [2], [3]. LFPs are known for their improved stability in chronic implant scenarios, and due to their lower frequency content, they hold the potential for substantial reductions in sampling and processing rates, thereby offering benefits in terms of power consumption.

LFPs are obtained by low-pass filtering (sub-300 Hz) the raw, wideband voltage recording from which spikes are also acquired, and reflect collective activity of the underlying neural population. These signals are coarser grain, but they present highly meaningful information for estimating patient's neural state or intentions [1], [4], [5]. Presently, there is scarcity of tools capable to exploit LFPs in real-time, as existing electrophysiology acquisition systems are limited to spike detection and sorting.

This work has been supported by the UK Engineering and Physical Sciences Research Council grant EP/R024642/1 (FORTE) and the EU commission H2020 programme no. 824165 (SYNCH).

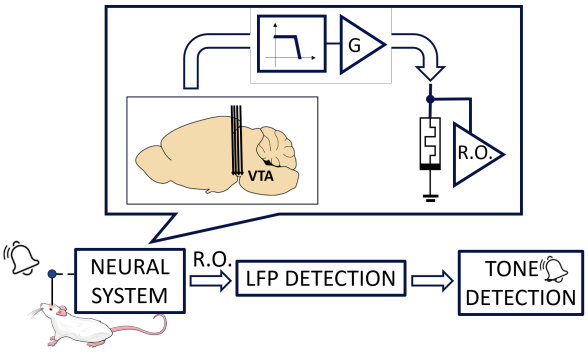

Fig. 1. LFP signal processing chain. The animal was implanted with a chronic monitoring probe. A single frequency tone was played, and the response acquired using a neural acquisition system. The acquired data was conditioned to isolate the LFP components and match the voltage dynamic of the RRAM. The RRAM was directly stimulated by LFP signal, and its resistance was measured. LFP patterns were detected identifying significant changes in RRAM resistive state, thus detecting tones.

A rapidly emerging way to process neural signals is using memristive devices. Resistive Random Access Memories (RRAMs) are two terminal elements, where the formation/disruption of a voltage-driven conductive filament modulates the device resistance. They exhibit thresholding and integrating behaviours, which are attractive for detecting signal patterns in spikes and LFPs. Previous works like [6], [7], have shown RRAMs can be used for spike detection and sorting and recently 1 transistor - 1 RRAM (1T1R) arrays have been used for LFP processing [8].

In this paper we present a modified Memristive Integrating Sensor (MIS) approach [6], for detecting LFP events. MIS shows how RRAM can successfully encode and compress spiking events, offering a competitive balance between detection accuracy and power consumption. The main goal of this study is to explore the possibility of utilizing LFPs to detect significant external stimuli and we assess the performance of this method towards real-time detection.

The document is organised as follows: section II presents the platform that we implemented to apply the signals to RRAM, giving details about the devices and the in-vivo neural recording we used to test our methodology. In Section III

we present the results obtained relying on such experimental set-up and discuss the data thresholding strategy, and real-time stimulation detection based on RRAM response to LFP signals. In section IV a summary of the key findings and their broader implications is provided.

II. Materials and Methods

A. High-level description

The concept of our experiment is outlined in Figure 1. Here, we used pre-recorded activity from a rat. The activity was recorded with chronically implanted electrode array, allowing continuous monitoring of neural activity from freely moving animals [9]. During the experiment, broadband extracellular activity in the Ventral Tegmental Area (VTA) of the rat was recorded while a single frequency sound was played.

The neural activity, band-pass filtered and amplified, was fed to the RRAM device. The band-pass in 1–100 Hz range allowed us to eliminate any offset and to remove high-frequency components. A gain in the order of 10^4 was needed, to scale the input voltage (which has a maximum range of $\pm 50\ \mu V$) to a level compatible with the switching threshold of the RRAM, V_{th}, ranging between $2.8 - 3.2$ V.

The pre-processed waveform was then applied directly to a RRAM device. Here, whenever the input V was greater than V_{th}, the RRAM resistive state (RS) changed in a non-volatile fashion [10]. While the LFPs were applied to the device, its state was also monitored, and the conductance values were transferred to a PC. By analysing the time evolution of the RRAM resistance in real-time, patterns within the LFP trace corresponding to the played tone stimulation could highlighted. Further details on the platform implementation are provided in Section II-D.

Notably, LFP data exhibit variations that are more symmetrical in the positive and negative polarities with respect to spikes. This characteristic lead to the occurrence of SET (lowest resistive state) and RESET (highest resistive state) states in the RRAM in an alternating manner. Consequently, unlike other works, there was no requirement for external resetting pulses [6]. Also, with respect to spike processing, the sampling frequency used to feed the neural signal to the RRAM, could be strongly reduced down to 500 Hz, and even beyond. This benefit added to the one offered by the RRAM, which intrinsically acts as a memory stage, therefore enabling us to access the neural activity less often.

B. RRAM devices

The experiments were performed using solid-state titania/alumina-based devices with vertical stack structure (from bottom to top): Pt/TiO_{2-x}/AlO_x/Pt fabricated on SiO_2/Si substrates using reactive magnetron sputtering in Ar/O_2 ambient (for the dielectrics) and e-beam evaporation (for the metals). Depending on the choice of materials the devices can operate in either binary ($R_{\text{on}}/R_{\text{off}} > 10$), or in a smoother analogue fashion as per [10]. For the sake of this experiment the analogue non-volatile behaviour was preferred.

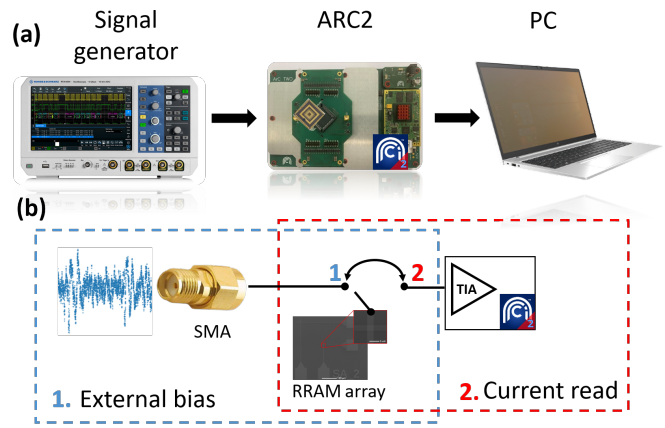

Fig. 2. Experimental set-up. (a) The amplified LFP trace was replayed by a signal generator and fed to the ARC TWO daughter-board hosting the RRAM devices. Data acquired from ARC TWO were streamed to a PC for processing. (b) The ARC TWO daughter-board was equipped with switches that alternated between two states: 1) RRAM biased by the signal generator, and 2) RRAM connected to the read-out internal circuit of ARC TWO for resistance reading. These switches effectively downsampled the 40 kHz input to 500 Hz.

C. Neural data collection

Biological experiments were performed at Bar-Ilan University. All procedures were approved by the Bar-Ilan University Institutional Animal Care and Use Committee. Prior to experiments, the animals underwent a surgical procedure during which sixteen microwires (35 µm, isonel coated tungsten; California Fine Wire Company) arranged in 4×4 arrays were lowered into the brain and fixed in position using dental cement. During the experiment, broadband neural activity was amplified and continuously sampled at 40 kHz using a multi-channel neuronal recording data acquisition system (OmniPlex, Plexon Inc) [11]. Nine recording channels out of the sixteen contained activity and were further analysed. The recorded channels exhibited a significant level of correlation, and we identified a channel with best signal-to-noise-ratio. From the selected recording, we extracted snippets corresponding to tone stimulation, followed by a few seconds of basal activity. These snippets were then assembled into a trace, forming the basis for our experimental analysis.

D. Experimental set-up

Figure 2 illustrates the implementation of the concept from Section II-A. The data were filtered using MATLAB software, and replayed with a ROHDE & SCHWARTZ signal generator at a sampling frequency of 40 kHz. A gain factor was applied by the signal generator to get max peak-to-peak of around 6.4 V. The signal was applied to the RRAM through an ARC TWO board [12], a stand-alone, desktop-controlled system, hosting the devices-under-test (DUT) on a daughter-board (DB) equipped with a subminiature A (SMA) connector to transmit the LFP signal to the RRAM.

The DB was regulated by switches that alternated the connection of the DUT between two configurations: 1) LFP signal lines via SMA, and 2) read-out circuitry on ARC TWO

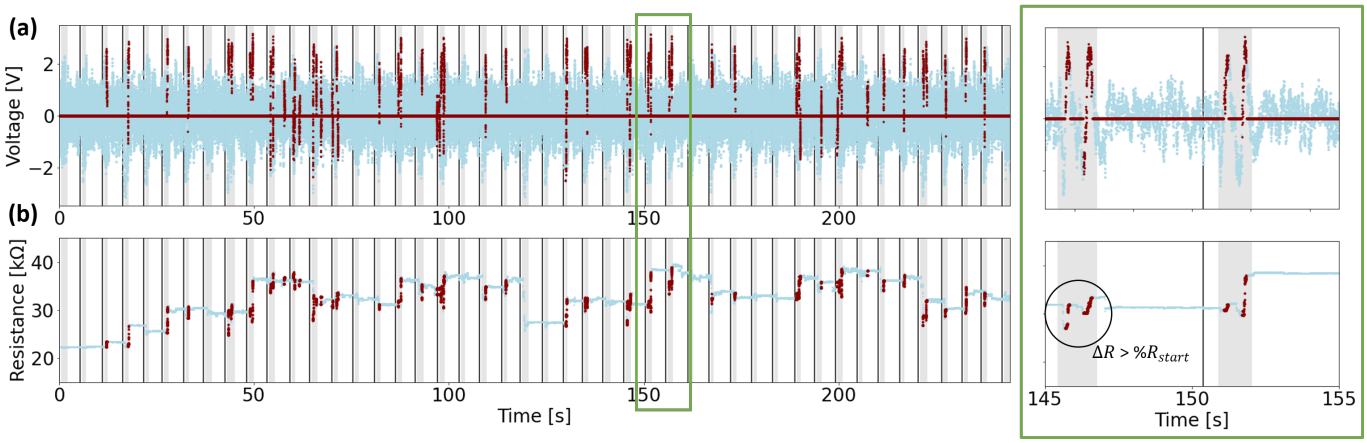

Fig. 3. Response of an RRAM device to an LFP neural recording. (a) One-channel extracellular recording acquired in the VTA, band-pass filtered 1–100 Hz and amplified by a factor of 6.4×10^4 to match with the RRAM voltage dynamics. Black vertical lines denote stimulus presentation (a musical note played to the awake animal). Grey boxes frame areas of the neural signal in which we actually observed variation of the LFP activity, induced by the tone stimulation. (b) RRAM response to the neural signal. The resistive state of the RRAM was acquired after every sample of the trace is applied. The signal was applied with a frequency of 500 Hz, same for read-out frequency. Read-outs were grouped into batches of 70 values. By applying a simple thresholding condition on the RRAM response it was possible to detect the boxed areas of the LFP trace. In both graphs, red batches represent supra threshold batches (in this case $R_{\text{start, bc}}$ - $R_{\text{end, bc}} > 2\% R_{\text{start, bc}}$, indicating the detection of a meaningful area.

implemented by a trans-impedance amplifier. Figure 2b depicts this protocol. During phase 1, a voltage-read circuit on the ARC TWO board was also used to record the input signal applied to the devices, which made it simple to align the stimulus with RRAM response. By adjusting the toggling frequency of the switches, the sampling frequency for the RRAM stimulation was tuned, enabling us to down-sample the received input. In our experiment the complete switches cycle duration was 2 ms, with the RRAM being biased by the LFP for 400 μs and subsequently read by applying a default read voltage (0.5 V). The read operation itself took approximately 1.5 ms. This sets the biasing frequency of the RRAM at 500 Hz. Acquisition of the top graph involved employing the internal voltage read circuit on the ARC TWO board, which records the input signal applied to the devices.

RRAM read-outs were obtained in batches of 70 values, corresponding to the maximum storage capacity of the internal FPGA instruction buffer controlling ARC TWO. These read-out batches were subsequently transmitted to a PC for real-time analysis. Each batch had a duration of approximately 140 ms, with a read-out performed every 2 ms. This duration aligned well with interesting variations in the LFP, such as those caused by external stimuli. Consequently, the software analysis following each read-out was conducted on a batch-by-batch basis, taking advantage of the temporal dynamics that match closely, and enabling the detection of high-amplitude LFP signals that corresponded to stimulations applied to the animal.

III. Data Processing and Results

The processing and analysis is structured into two main parts. In the first part, we investigate the experimental data to determine the optimal strategy for processing the resistive changes and extracting meaningful patterns. Key parameters, including threshold criterion and observation window, are established during this phase. In the second part, based on the observations from the previous analysis, we propose a real-time solution for detecting stimulation-induced LFP changes.

A. Detection and thresholding

Figure 3 displays the data of an experiment ran with the earlier described methodology. The top trace illustrates the signal applied to the RRAM and the bottom trace represents the corresponding resistive state throughout the experiment. Tone stimulation events are represented on both plots by black vertical lines, while grey boxes highlight areas where LFP activity is correlated with the external stimulation. Focusing on the bottom graph, we see the main RRAM resistive drops happened within the grey boxes, reveling the overall RRAM's reactivity to significant LFP events, while presenting good filtering action to minor fluctuations. To detect meaningful resistance changes, we conducted an investigation to select an appropriate thresholding strategy. As described in Section II-D, the RRAM readings were obtained in batches of 70 values, enabling batch-by-batch online analysis. Initially, we compared the maximum resistive variation between adjacent points within each batch to a resistance threshold, denoted as R_{th}. Above-threshold points were interpreted as stimulus events. This is identified as Strategy 1A in Table I. Two variations of this approach were also considered, where respectively the condition was applied to the absolute value of ΔR (1B), and subsequently where the threshold value is not a fixed value, but a percentage of the resistive state at the beginning of the batch $R_{\text{start, bc}}$ (1C). To make the computation more efficient, we then chose a bolder approach, and took into consideration only the the first and the last resistive value within the batch, $R_{\text{start, bc}}$ and $R_{\text{end, bc}}$. Here, we considered the resistive drops $R_{\text{start, bc}} - R_{\text{end, bc}}$, and compared

TABLE I
THRESHOLD STRATEGIES

Strategy Name	Threshold
1A	$max((diff(R)) > R_{th}$
1B	$max(abs(diff(R))) > R_{th}$
1C	$max(diff(R)) > \%R_{start,bc}$
2A	$R_{start,bc} - R_{end,bc} > R_{th}$
2B	$R_{start,bc} - R_{end,bc} > \%R_{start,bc}$
3	$R_{max,bc} - R_{min,bc} > \%R_{min,bc}$

them initially to R_{th} (Strategy 2A), and then to $\%R_{\text{start, bc}}$ (2B). This approach offers hardware optimization benefits by enabling further downsampling and eliminating the need for storing and shifting intermediate data to track maximum or minimum resistive drops. Additionally, we explored a strategy that involves accessing the maximum and minimum resistance values within a batch (Strategy 3), trying to check whether it performs any worse than the more hardware friendly approach of start end.

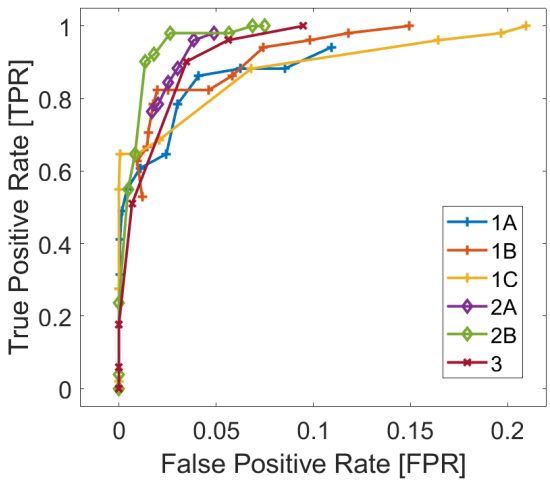

Fig. 4. Comparison of Receiver Operating Characteristic (ROC) curves for different thresholding conditions. RRAM state read-outs are processed in batches, and a thresholding condition is applied to each batch to identify significant events. Various threshold strategies are evaluated, and the ROC curve for each strategy is plotted. The strategy that produces the best performing ROC curve is given by approach 2B.

The performance of these criteria was analyzed by plotting the Receiving Operating Characteristic (ROC) curves, Fig. 4. Among them, criteria 2B, comparing the $R_{start,bc}$ - $R_{end,bc}$ drop to the resistance at the beginning of the batch, demonstrated superior performance. Areas of supra-threshold activity in the experiment are highlighted in red in Figure 3.

B. Towards real-time detection

However, during LFP events identified by grey areas in Fig. 3, there were instances where multiple consecutive batches surpassed the threshold due to the prolonged duration of an LFP event (which could last up to 200–300 ms, while each batch was 70 ms). This can be problematic for real-time detection as it inflates the number of false positives

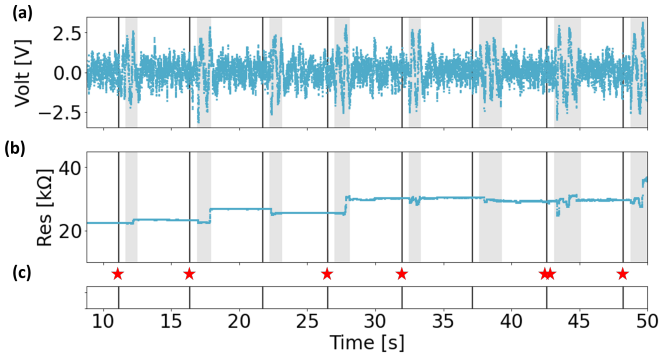

Fig. 5. Real-time detection of LFPs. (a) The neural signal applied to the RRAM; (b) corresponding RRAM threshold crossings that were monitored and stored for every batch of 70 values, using threshold strategy 2B, identified in Fig. 4, and a threshold of $2\%R_{start,bc}$. Aggregations of ten consecutive batches were scanned, and if at least one crossing was observed, a stimulation was detected; (c) red stars indicate a detected event, while ground truth is represented by black vertical lines.

which need to be minimised in order to achieve reliable near real-time detection. Expanding on threshold strategy 2B, which was previously applied to individual batches, we now encompassed a larger time window, consisting of X non-overlapping, consecutive batches. Within this *superbatch*, we counted the number N of instances that crossed the threshold, and established a second cut-off condition. Essentially, if the *rate of threshold crossings*, $[(N \text{ crossings})/(X \text{ batches})]$, was greater than a chosen minimum rate, M, then an LFP event was detected. By implementing this approach, the detection remained consistent as a single event, even when there were multiple crossings within X consecutive batches. Figure 5 shows a snapshot of the real-time detection process, where in (c) we compare the presence of the external tone stimulation in black, with our detections, represented by red stars. Here, the threshold was set at 2% of $R_{start,bc}$, which gave best TPR-FPR balance. Setting $M = 1$, and $X = 7$, and running the detection process, we got an accuracy of 85%, with a minimized FPR of 1.5%.

IV. CONCLUSIONS

To summarise, we presented a method to efficiently process and detect LFP signals using a RRAM-based setup. LFP traces were downsampled and applied to RRAM devices while their response was monitored. Depending on the thresholding strategy applied, we were able to tune the accuracy of the process and minimise the false positive rate. By expanding the time domain of the process, we achieved near real-time detection of LFP events.

Although LFPs offer unique balance between granularity, stability in chronic acquisition, and variation speed, adequate methods or techniques for their online monitoring are still missing. Our approach offers a unique capability to seamlessly interface RRAM with analogue neural signals in a MIS fashion, opening the way to provide neuroscience with a new tool to perform real-time tracking of LFP events.

REFERENCES

[1] N. Even-Chen, D. G. Muratore, S. D. Stavisky, L. R. Hochberg, J. M. Henderson, B. Murmann, and K. V. Shenoy, "Power-saving design opportunities for wireless intracortical brain–computer interfaces," *Nature Biomedical Engineering*, vol. 4, no. 10, p. 984–996, Aug. 2020. [Online]. Available: http://dx.doi.org/10.1038/s41551-020-0595-9

[2] S. D. Stavisky, J. C. Kao, P. Nuyujukian, S. I. Ryu, and K. V. Shenoy, "A high performing brain–machine interface driven by low-frequency local field potentials alone and together with spikes," *Journal of Neural Engineering*, vol. 12, no. 3, p. 036009, May 2015. [Online]. Available: http://dx.doi.org/10.1088/1741-2560/12/3/036009

[3] A. Jackson and T. M. Hall, "Decoding local field potentials for neural interfaces," *IEEE Transactions on Neural Systems and Rehabilitation Engineering*, vol. 25, no. 10, p. 1705–1714, Oct. 2017. [Online]. Available: http://dx.doi.org/10.1109/TNSRE.2016.2612001

[4] S. R. John, W. Dagash, A. N. Mohapatra, S. Netser, and S. Wagner, "Distinct dynamics of theta and gamma rhythmicity during social interaction suggest differential mode of action in the medial amygdala of sprague dawley rats and C57BL/6J mice," *Neuroscience*, vol. 493, p. 69–80, Jun. 2022. [Online]. Available: http://dx.doi.org/10.1016/j.neuroscience.2022.04.020

[5] D. Gervasoni, S.-C. Lin, S. Ribeiro, E. S. Soares, J. Pantoja, and M. A. L. Nicolelis, "Global forebrain dynamics predict rat behavioral states and their transitions," *The Journal of Neuroscience*, vol. 24, no. 49, p. 11137–11147, Dec. 2004. [Online]. Available: http://dx.doi.org/10.1523/JNEUROSCI.3524-04.2004

[6] I. Gupta, A. Serb, A. Khiat, R. Zeitler, S. Vassanelli, and T. Prodromakis, "Sub 100 nw volatile nano-metal-oxide memristor as synaptic-like encoder of neuronal spikes," *IEEE Transactions on Biomedical Circuits and Systems*, vol. 12, no. 2, p. 351–359, Apr. 2018. [Online]. Available: http://dx.doi.org/10.1109/TBCAS.2018.2797939

[7] C. Dias, D. Castro, M. Aroso, J. Ventura, and P. Aguiar, "Memristor-based neuromodulation device for real-time monitoring and adaptive control of neuronal populations," *ACS Applied Electronic Materials*, vol. 4, no. 5, p. 2380–2387, May 2022. [Online]. Available: http://dx.doi.org/10.1021/acsaelm.2c00198

[8] Z. Liu, J. Tang, B. Gao, X. Li, P. Yao, Y. Lin, D. Liu, B. Hong, H. Qian, and H. Wu, "Multichannel parallel processing of neural signals in memristor arrays," *Science Advances*, vol. 6, no. 41, Oct. 2020. [Online]. Available: http://dx.doi.org/10.1126/sciadv.abc4797

[9] Y. Baumel and D. Cohen, "State-dependent entrainment of cerebellar nuclear neurons to the local field potential during voluntary movements," *Journal of Neurophysiology*, vol. 126, no. 1, p. 112–122, Jul. 2021. [Online]. Available: http://dx.doi.org/10.1152/jn.00551.2020

[10] C. Wang, Z. Si, X. Jiang, A. Malik, Y. Pan, S. Stathopoulos, A. Serb, S. Wang, T. Prodromakis, and C. Papavassiliou, "Multi-state memristors and their applications: An overview," *IEEE Journal on Emerging and Selected Topics in Circuits and Systems*, vol. 12, no. 4, p. 723–734, Dec. 2022. [Online]. Available: http://dx.doi.org/10.1109/JETCAS.2022.3223295

[11] N. D. Peer, H. G. Yamin, and D. Cohen, "Multidimensional encoding of movement and contextual variables by rat globus pallidus neurons during a novel environment exposure task," *iScience*, vol. 25, no. 9, p. 105024, Sep. 2022. [Online]. Available: http://dx.doi.org/10.1016/j.isci.2022.105024

[12] P. Foster, J. Huang, A. Serb, S. Stathopoulos, C. Papavassiliou, and T. Prodromakis, "An FPGA-based system for generalised electron devices testing," *Scientific Reports*, vol. 12, no. 1, Aug. 2022. [Online]. Available: http://dx.doi.org/10.1038/s41598-022-18100-3